Eur. Phys. J. Appl. Phys. **98**, 20 (2023)

https://doi.org/10.1051/epjap/2023220270

THE EUROPEAN PHYSICAL JOURNAL APPLIED PHYSICS

Special Issue on 'Amorphous alloys and multiscale materials: Fundamental aspects and Energy applications', edited by Zhao Zhankui, Wang Hongli and Tai Cheuk-Wai

Regular Article

Effect of stress relaxation on soft magnetic properties of $Fe_{76}Si_9B_{10}P_5$ metallic glass

Yurong Gao[1,2,a], Yu Tong[1,a], Lijian Song[1,*], Jiacheng Liu[3], Bowen Zang[1], Mingliang Xiang[1], Meng Gao[1], Yan Zhang[1], Juntao Huo[1], and Jun-Qiang Wang[1]

[1] CAS Key Laboratory of Magnetic Materials and Devices, Zhejiang Province Key Laboratory of Magnetic Materials and Application Technology, Ningbo Institute of Materials Technology and Engineering, Chinese Academy of Sciences, Ningbo 315201, P.R. China
[2] School of Materials Science and Chemical Engineering, Ningbo University, Ningbo 315211, P.R. China
[3] Ningbo Institute of Materials Technology and Engineering, Chinese Academy of Sciences, Ningbo 315201, P.R. China

Received: 29 October 2022 / Received in final form: 10 December 2022 / Accepted: 10 January 2023

Abstract. Stress relief can improve the soft magnetic properties of Fe-based metallic glasses (MGs) and is vital for industrial applications. In this work, we investigated the evolution of soft magnetic properties, relaxation dynamics, and mechanical properties of Fe-based MGs under different applied tensile strains and stress relaxation times. We found that stress relaxation can significantly reduce coercivity H_c by 95% compared with as-quenched state. Furthermore, the coercivity H_c, apparent activation volume V_{act} and time constant t_r all show analogous two-stage variation with annealing time, accompanied by approximate crossovers. This suggests that the microstructure change emerges, further verified by the domain wall motion and the transition from elastic to plastic. These results are helpful in preparing Fe-based MGs with excellent soft magnetic and mechanical properties by controlling the stress relaxation condition.

1 Introduction

Fe-based metallic glasses (MGs) with special disordered atomic structure and composition are widely used in core materials for distribution systems because they have a high saturated magnetic flux density, low coercivity, high permeability, good mechanical properties, and low production cost [1–5]. They are excellent new materials for energy saving and environmental protection. However, the metallic glasses stay out equilibrium state due to the internal stress trapped in the MGs during rapid quenching process [6–8]. From the perspective of structural defects, the residual stress reflects the point (free volume) or liner defects (quasi-dislocation dipoles), all of them will influence the magnetic properties [9,10].

To improve the magnetic properties of Fe-based MGs, extensive investigations have been performed to release the quenched-in stress upon the annealing process [5,11–14]. Generally, the stress relaxation can decrease the coercivity H_c, enhances the magnetization strength and favor the domain wall motion [15,16]. However, deep relaxation deteriorates the mechanical properties of Fe-based MGs, limiting the practical application [5,7]. Recently, two-step relaxations, from fast process to slow process, were built in the stress relaxation of MGs below glass transition temperature [17–19]. The stress-driven fast relaxation maintains the mechanical properties in nature, while the thermal-driven slow relaxation triggers the plastic flow events [5,19–22]. However, the one-to-one relationship between stress relaxations and soft magnetic properties is still not clear.

In this work, we investigated the evolution of soft magnetic properties, relaxation dynamics, and mechanical properties of Fe-based MGs under different applied tensile strain and stress relaxation times. These results reveal that it is probable to prepare Fe-based MGs with excellent soft magnetic properties and plasticity by controlling the stress relaxation conditions.

2 Experimental

The $Fe_{76}Si_9B_{10}P_5$ (at.%) master alloy ingot was produced by induction melting the mixture of pure metals of Fe (99.99 wt.%), pure metalloid of crystal Si (99.99 wt.%) and B (99.99 wt.%), and pre-melted Fe_3-P (atomic ratio with purity of 99 wt.%) in an arc furnace under an argon atmosphere. The metallic glass ribbons were fabricated by the single-roller quenching method. The glass structure of as-quenched ribbons was identified by X-ray diffraction (XRD, Bruker D8 Advance) using Cu $K\alpha$ radiation. The glass transition temperature T_g was examined by

* e-mail: songlj@nimte.ac.cn
[a] These authors contributed equally to this work.

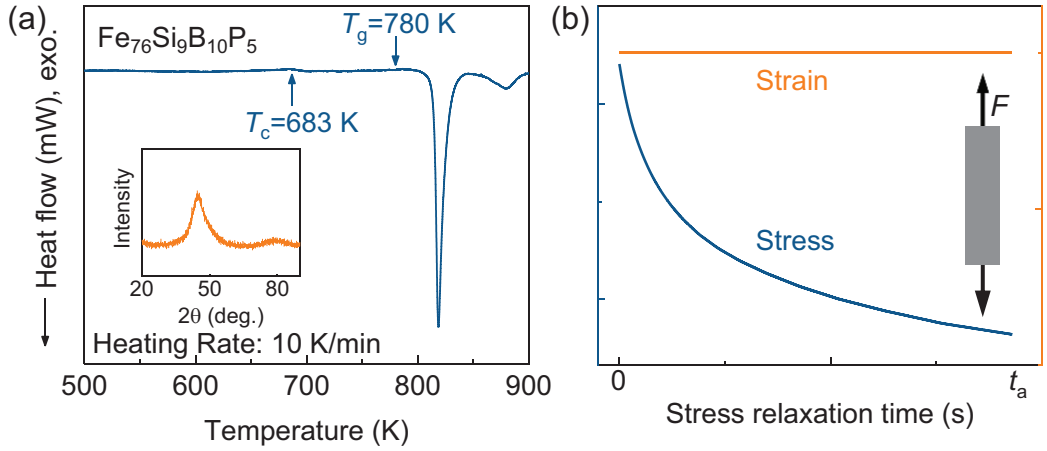

Fig. 1. (a) The DSC curve of the as-quenched $Fe_{76}Si_9B_{10}P_5$ MG ribbon at a heating rate of 10 K/min, and the glass transition temperature T_g is determined to be about 780 K. The inset is the XRD pattern of the as-quenched $Fe_{76}Si_9B_{10}P_5$ MG ribbon. (b) Stress and strain response versus time during stress relaxation experiments. The inset is the schematic image of tensile experiments in DMA, and a pair of equal and opposite forces are applied on both sides of the sample.

differential scanning calorimeter (DSC, Netzsch 404C) at a heating rate of 10 K/min under a constant flow (20 ml/min) of high-purity argon gas. The coercivity (H_c) of samples was measured by a DC *B-H* loop tracer (BHS-40S) under a magnetic field of 800 A/m. The *M-H* curves were performed by a superconducting quantum interference device magnetometer (SQUID) using Quantum Design MPMS. The magnetic domain structure was revealed by digitally enhanced 950MT magneto-optic Kerr microscope. The stress relaxation and strain recovery experiments were performed on a dynamic mechanical analyzer (DMA, TA instrument Q800) with ribbon samples.

3 Results and discussion

Figure 1a shows the DSC curve of the as-quenched $Fe_{76}Si_9B_{10}P_5$ MG ribbon at a heating rate of 10 K/min. There is a sharp exothermic peak presented in Figure 1a, which represents the crystallization of the alloy. Glass transition process could be observed prior to the crystallization process with a T_g determined at 780 K. The inset of Figure 1a presents the XRD pattern of the as-quenched $Fe_{76}Si_9B_{10}P_5$ MG ribbon, which shows only one broad peak and without any detectable sharp peaks. The XRD pattern indicates the fully amorphous nature of the as-quenched sample. The stress relaxation tests were carried out at 673 K in a nitrogen atmosphere using ribbon samples on DMA. Figure 1b shows the stress and strain response versus time during stress relaxation experiments. For the stress relaxation experiments, the samples were equilibrated for 5 min at the target experiment temperature. Then, the uniaxial tensile experiments were performed at different constant strains ε (= 0, 0.1%, 0.2%, 0.3% and 0.4%) for different times t_a (=30, 132, 600, 1800, 3480, 7200 s). The inset of Figure 1b presents the schematic diagram of the DMA tensile mode. Equal and opposite forces are applied to both sides of the sample to ensure uniform deformation in the test.

We measured the soft magnetic properties of all samples under different stress relaxation conditions. Figure 2a shows the evolution of coercivity H_c as a function of stress relaxation time with different applied strains ε at 673 K. For a given tensile strain ε, the H_c decreases with the extension of stress relaxation time t_a and reaches the minimum at t_a =1800 s. Further increasing the stress relaxation time slightly increases the H_c. The decrease of H_c is mainly attributed to stress relief by structural relaxation, which is similar to the situation where the magnetic properties change dramatically after 5–10 min of conventional annealing [13,23–26].The pre-longed annealing time required to achieve the minimum H_c might be due to the stress applied to the sample. Figure 2b shows the H_c of $Fe_{76}Si_9B_{10}P_5$ MG before and after stress relaxation under different strains for $t_a = 1800$ s. The H_c of as-quenched MG was reduced by 95% after stress-relaxation under 0.4% strain, from 13.56 A/m to 0.68 A/m. This indicates that the internal stress of the stress-relaxed samples was released sufficiently. Previous works have shown that slope of the domain wall motion region and the domain rotation region of the *M-H* curve represent the stress relief in Fe-based MGs [25,26]. Figure 2c shows the first quadrant of the hysteresis loops of an as-quenched sample (blue line) and a stress-relaxed sample ($T_a = 673$ K, $t_a = 1800$ s, $\varepsilon = 0.3\%$) (red line) acquired by SQUID. Compared to the as-quenched sample, the slope in the hysteresis loop of the stress-relaxed sample becomes gentler due to the stress relaxation process. The shape of hysteresis loop could also affect the coercivity. In order to study the changes in soft magnetic properties systematically, the magnetic domains of the representative samples were observed by using Magneto-optical Kerr Microscope (Fig. 2d). In the case of as-quenched samples, strong and non-uniform quenched-in stresses resist the ordered arrangement of magnetic domains, resulting in the maze-like domains. After stress relaxation for a short time below T_g, these internal stresses could be released because of the annihilation of low-energy barrier flow units, yielding in the variation of the domains

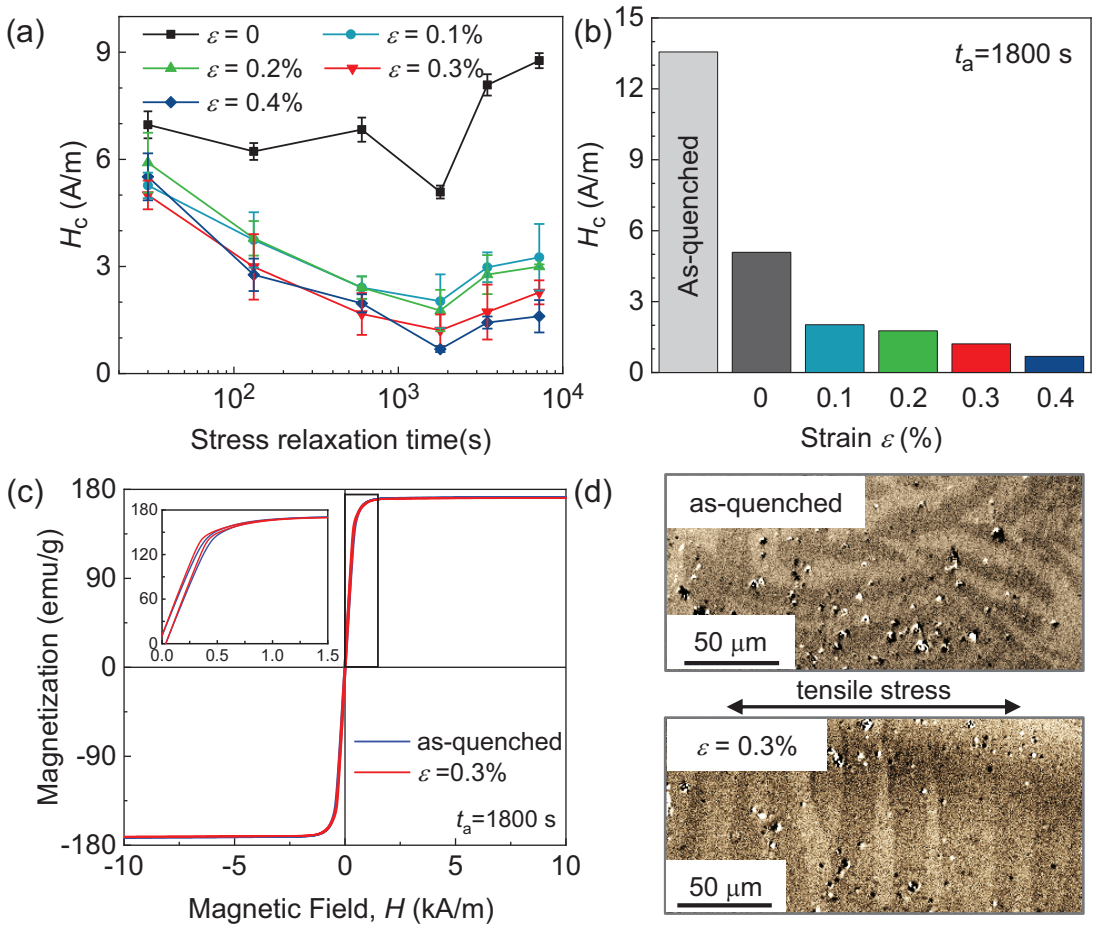

Fig. 2. (a) Relaxation time dependence of coercivity H_c after pre-relaxation under various strains ε at 673 K. (b) Comparison of coercivity H_c before and after stress relaxation for $t_a = 1800$ s. (c) Hysteresis loop of the as-quenched MG sample and the stress-relaxed sample at 673 K for 1800 s acquired by SQUID. (d) The domain structure of the as-quenched MG sample and the sample stress-relaxed at 673 K for 1800 s.

to regular patterns [25,27]. On the other hands, the H_c decreases with increasing of strain under the same stress relaxation time, reflecting an increasing stress relief rate with larger strain. However, when the stress relaxation time exceeded 1800 s, the value of coercivity showed an increasing trend with time.

For further understanding the underlying dynamics during stress relaxation, Figure 3a shows the stress drop $\Delta\sigma$ versus stress relaxation time with different strains for 7200 s at 673 K. The stress decreases rapidly from initial stress and then lessens slowly as time goes by, which implies that the strain rate increases with the increase of the applied strain ε. The relationship between stress and time during the stress relaxation process of MGs can be described by [28,29]:

$$\Delta\sigma(t) = \frac{-k_B T}{V_{\text{act}}} \ln\left(1 + \frac{t}{t_r}\right) \tag{1}$$

where the stress drop $\Delta\sigma\ (t) = \sigma(t) - \sigma(0)$ and $\sigma(0)$ is the initial stress applied, k_B is the Boltzmann constant, T is the experimental temperature, V_{act} is the apparent activation volume, t is the time variable, t_r is the time constant. According to equation (1), the values of the apparent activation volume V_{act} and the time constant t_r are given in Figures 3b and 3c, respectively. Our investigation presents that the change in the apparent activation volume V_{act} and the time constant t_r with relaxation time both consist of two stages, which is similar to the variation of coercivity H_c. In Figure 3b, the values of V_{act} have the maximum value at the start and then decrease with stress relaxation time until 1800 s. It means the stress relaxation mechanism becomes less collected at a longer time or under a bigger strain [30]. As time elapses, it shows an upward tendency after 1800 s, which is probably associated with the transition from a fast process to a slow process during stress relaxation for a sufficiently long time [17–19,31]. In addition, t_r increases with stress relaxation time before 1800 s, indicating that atomic mobility reduces and the difficulty of local atomic rearrangement increases [28]. After 1800 s, t_r decreases with stress relaxation time. That means the activation volume for plastic deformation increases with stress relaxation time and it can be activated faster at larger tensile strain than that at smaller tensile strain [28].

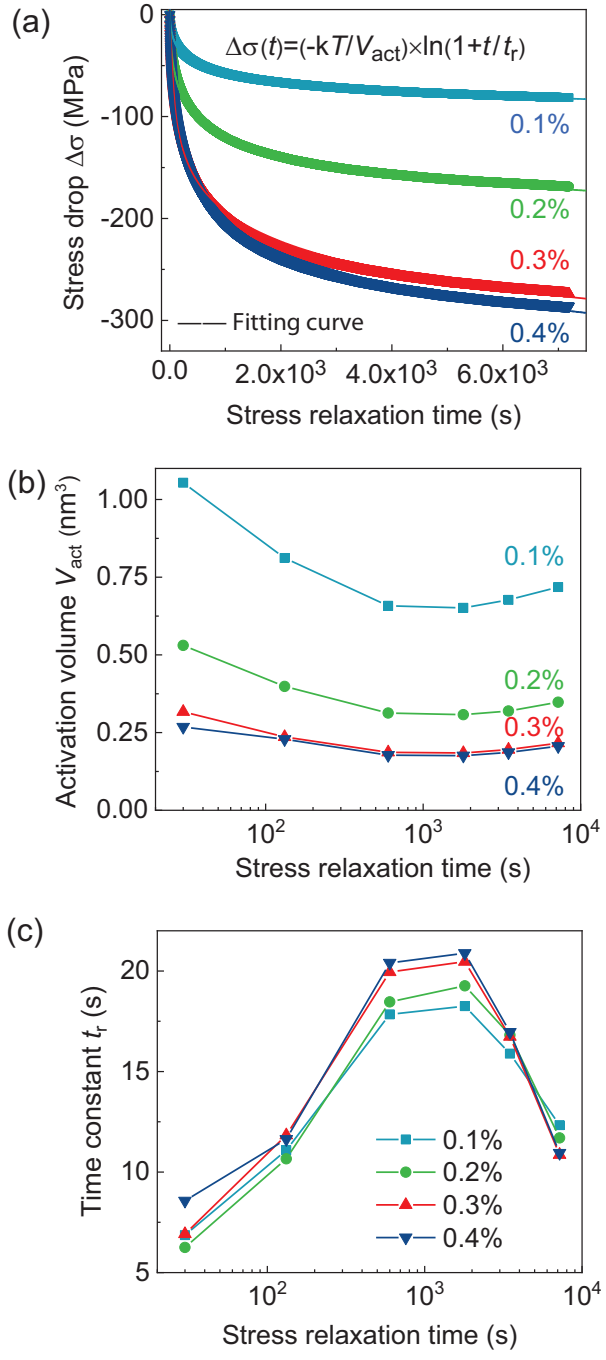

Fig. 3. (a) Comparison of the stress drop $\Delta\sigma$ with different applied strains ε for 7200 s at 673 KB. The fitting parameters V_{act} (b) and t_r (c) of $Fe_{76}Si_9B_{10}P_5$ MG as a function of stress relaxation time.

The mechanical behavior of MGs is related to their internal structural heterogeneity, which is composed of multiple liquid-like zones (flow units) and stiffer surroundings (elastic matrix). To understand the mechanism of the two-stage stress relaxation process, we analyzed the strain recovery behavior after different stress relaxation times. Figure 4 shows the representative strain recovery curves after stress relaxation for 600 s and 3480 s, respectively. The deformation behavior during strain recovery experiments can be divided into three parts. The elastic strain ε_e and plastic strain ε_p are the recoverable instantaneous and non-recoverable parts of the residual strain, respectively [20,22,32]. The anelastic strain ε_a denotes the slow recovery component of residual strain, and the corresponding relaxation curves can be well fitted by the KWW function [20,32]:

$$\frac{(\varepsilon_t - \varepsilon_p)}{(\varepsilon_0 - \varepsilon_p)} = \exp\left(-\frac{t}{\tau_c}\right)^{\beta_{KWW}} \quad (2)$$

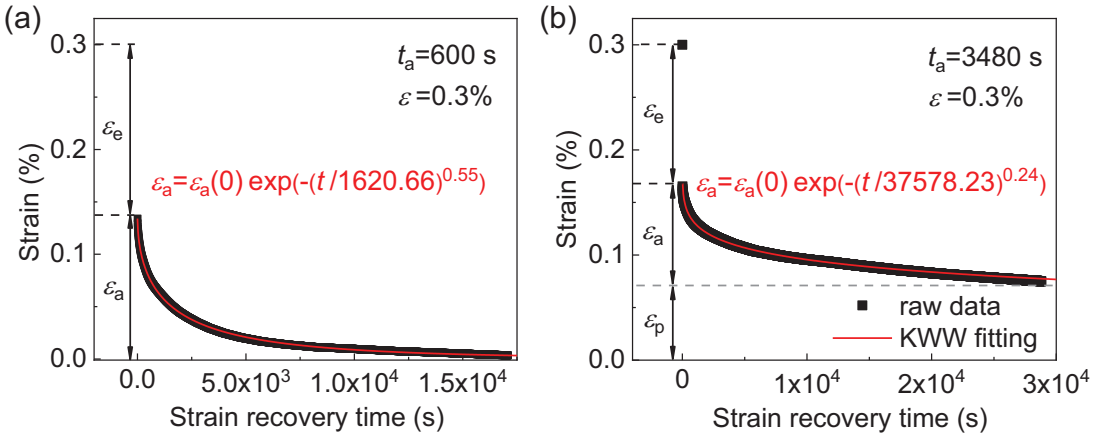

Fig. 4. The strain recovery process after the stress relaxation process lasts for 600 s (a) and 3480 s (b), the recovered strain ε_a fitted by the KWW equation respectively.

where ε_p is the plastic strain, ε_0 is the initial strain, τ_c is the average relaxation time, and β_{KWW} is a non-exponential parameter. After stress relaxation for 600 s, which is ahead of the appearance of crossover in Figures 2a and 3, the recovery data can be well fitted by the $\varepsilon_a = \varepsilon_a(0)\exp(-(t/1620.66)^{0.55})$, indicating that plastic strain ε_p is approaching to zero. The residual strain was fully recovered after a short recovery time and only elastic deformation occurred in the fast process, as shown in Figure 4a. It is widely recognized that stochastic deformation units are activated, and localized shear transformation events are recoverable in the elastic regime of MGs [20,33]. For a long-time stress relaxation $t_a = 3480$ s, which is after the crossover points, the anelastic recovery data for 28800 s can be well fitted by the $\varepsilon_a = \varepsilon_a(0)\exp(-(t/37578.23)^{0.24})$ with a residual strain ε_p is up to 0.075%, as exhibited in Figure 4b. It reflects that plastic strain emerges due to the appearance of the slow process. Obviously, the slow process is related to the irreversible atomic rearrangements, representing that the localized deformation units self-organize and operate in a cooperative manner [34,35]. So the soft magnetic properties will deteriorate slightly in Figure 2a, resulting from the appearance of plastic strain in the slow process.

4 Conclusion

In summary, the relevance of soft magnetic properties and relaxation dynamics were investigated in $Fe_{76}Si_9B_{10}P_5$ metallic glass by stress relaxation. We found a crossover of relaxation dynamics from the fast process consistent with individual localized shear transformation process to the slow process consistent with the cooperative motion of localized deformation units emerging in stress relaxation. In the fast process, the soft magnetic properties are significantly improved, including the coercivity H_c declining sharply, and the magnetic domain walls becoming regular because of the stress relief. However, the soft magnetic properties deteriorate slightly due to the appearance of plastic strain in the slow process. These results reveal that it is probable to prepare Fe-based MGs with excellent soft magnetic properties and mechanical properties by controlling the stress relaxation condition.

The authors declare that they have no known competing financial interests or personal relationships that could have appeared to influence the work reported in this paper.

We acknowledge financial support from the National Key R&D Program of China (2018YFA0703600), National Natural Science Foundation of China (NSFC51922102, 52001319, 92163108, 52201193), Zhejiang Provincial Natural Science Foundation of China (LGF22E010002, LZ22A030001, LR22E010004), "Pioneer and Leading Goose" R&D Program of Zhejiang (2022C01023), Ningbo Key Scientific and Technological Project (2019B10051). The Natural Science Foundation of Ningbo City (No. 20221JCGY010142).

Author contribution statement

All the authors participated in this work. The preparation and characterization experiments, the data analysis and interpretation of the results were performed by Yurong Gao, Yu Tong, Lijian Song, Jiacheng Liu, Bowen Zang, Mingliang Xiang, Meng Gao, Yan Zhang, Juntao Huo, Jun-Qiang Wang. The manuscript was written and revised by Yurong Gao, Yu Tong, Lijian Song and Jun-Qiang Wang.

References

1. C. Suryanarayana, A. Inoue, Int. Mater. Rev. **58**, 131 (2013)
2. A. Makino, T. Kubota, C. Chang, M. Makabe, A. Inoue, Mater. Trans. **48**, 3024 (2007)
3. F. Wang, A. Inoue, Y. Han, F.L. Kong, S.L. Zhu, E. Shalaan, F. Al-Marzouki, A. Obaid, J. Alloys Compd. **711**, 132 (2017)
4. A. Inoue, B. Shen, Mater. Trans. **43**, 766 (2002)
5. N.N. He, L.J. Song, W. Xu, J.T. Huo, J.-Q. Wang, R.-W. Li, J. Non-Cryst. Solids **509**, 95 (2019)

6. P.G. Debenedetti, F.H. Stillinger, Nature **410**, 259 (2001)
7. W.H. Wang, Prog. Mater. Sci. **57**, 487 (2012)
8. W.L. Johnson, M.D. Demetriou, J.S. Harmon, M.L. Lind, K. Samwer, MRS Bull. **32**, 644 (2011)
9. L. Zhu, S.S. Jiang, Z.Z. Yang, G.B. Han, S.S. Yan, Y.G. Wang, J. Magn. Magn. Mater. **519**, 167513 (2021)
10. M. Nabiaek, M. Szota, M. Dospia, P. Pietrusiewicz, S. Walters, J. Magn. Magn. Mater. **322**, 3377 (2010)
11. M.C. Ri, D.W. Ding, B.A. Sun, J.Q. Wang, X.S. Zhu, B.B. Wang, T.L. Wang, Q.Q. Qiu, L.S. Huo, W.H. Wang, J. Non-Cryst. Solids **495**, 54 (2018)
12. S. Ouyang, L.J. Song, Y.H. Liu, J.T. Huo, J.-Q. Wang, W. Xu, J.L. Li, C.T. Wang, X.M. Wang, R.-W. Li, Phys. Rev. Mater. **2**, 063601 (2018)
13. P. Chen, T. Liu, F. Kong, A. Wang, C. Yu, G. Wang, C. Chang, X. Wang, J. Mater. Sci. Technol. **34**, 793 (2018)
14. M.C. Ri, D.W. Ding, S. Sohrabi, B.A. Sun, W.H. Wang, J. Appl. Phys. **124**, 165108 (2018)
15. F.E. Luborsky, J.L. Walter, Mater. Sci. Eng. **35**, 255 (1978)
16. F. Luborsky, J. Becker, J. Walter, H. Liebermann, IEEE. Trans. Magn. **15**, 1146 (1979)
17. J.C. Qiao, Y.J. Wang, L.Z. Zhao, L.H. Dai, D. Crespo, J.M. Pelletier, L.M. Keer, Y. Yao, Phys. Rev. B **94**, 104203 (2016)
18. P. Luo, P. Wen, H.Y. Bai, B. Ruta, W.H. Wang, Phys. Rev. Lett. **118**, 225901 (2017)
19. Y.R. Gao, Y. Tong, L.J. Song, X.X. Shui, M. Gao, J.T. Huo, J.Q. Wang, Scripta Mater. **224**, 115114 (2023)
20. W. Jiao, B.A. Sun, P. Wen, H.Y. Bai, Q.P. Kong, W.H. Wang, Appl. Phys. Lett. **103**, 081904 (2013)
21. L. Shao, L. Xue, J. Qiao, Q. Wang, Q. Wang, B. Shen, Scripta Mater. **222**, 115017 (2023)
22. Y.J. Duan, L.T. Zhang, T. Wada, H. Kato, E. Pineda, D. Crespo, J.M. Pelletier, J.C. Qiao, J. Mater. Sci. Technol. **107**, 82 (2022)
23. D. Azuma, R. Hasegawa, S. Saito, M. Takahashi, J. Appl. Phys. **113**, 17A339 (2013)
24. A. Inoue, R.E. Park, Mater. Trans., JIM **37**, 1715 (1996)
25. C. Wang, A. He, A. Wang, J. Pang, X. Liang, Q. Li, C. Chang, K. Qiu, X. Wang, Intermetallics **84**, 142 (2017)
26. J. Pang, A. Wang, S. Yue, F. Kong, K. Qiu, C. Chang, X. Wang, C.-T. Liu, J. Magn. Magn. Mater. **433**, 35 (2017)
27. G. Herzer, S. Flohrer, C. Polak, IEEE. Trans. Magn. **46**, 341 (2010)
28. Y. Tong, J.C. Qiao, C. Zhang, J.M. Pelletier, Y. Yao, J. Non-Cryst. Solids **452**, 57 (2016)
29. X.-S. Yang, Y.-J. Wang, G.-Y. Wang, H.-R. Zhai, L.H. Dai, T.-Y. Zhang, Acta Mater. **108**, 252 (2016)
30. Z.R. Xu, D.S. Yang, J.C. Qiao, J.M. Pelletier, D. Crespo, E. Pineda, Y.-J. Wang, Intermetallics **125**, 106922 (2020)
31. C. Zhang, L.H. Cai, B.H. Guo, B. Miao, J. Xu, Chin. J. Polym. Sci. **46**, 1 (2023)
32. Y.Z. Li, L.Z. Zhao, C. Wang, Z. Lu, H.Y. Bai, W.H. Wang, J. Appl. Phys. **118**, 154904 (2015)
33. J.S. Harmon, M.D. Demetriou, W.L. Johnson, K. Samwer, Phys. Rev. Lett. **99**, 135502 (2007)
34. Z. Wang, B.A. Sun, H.Y. Bai, W.H. Wang, Nat. Commun. **5**, 6823 (2014)
35. H.B. Yu, K. Samwer, W.H. Wang, H.Y. Bai, Nat. Commun. **4**, 2204 (2013)

Cite this article as: Yurong Gao, Yu Tong, Lijian Song, Jiacheng Liu, Bowen Zang, Mingliang Xiang, Meng Gao, Yan Zhang, Juntao Huo, and Jun-Qiang Wang, Effect of stress relaxation on soft magnetic properties of $Fe_{76}Si_9B_{10}P_5$ metallic glass, Eur. Phys. J. Appl. Phys. **98**, 20 (2023)